Band mixing effects in one-dimensional charge transfer insulators

Samuel Milner,[1] Steven Johnston,[2,3] and A. E. Feiguin[1]

[1] *Physics Department, Northeastern University, Boston, MA 02115, USA*
[2] *Department of Physics and Astronomy, The University of Tennessee, Knoxville, Tennessee 37996, USA*
[3] *Institute for Advanced Materials and Manufacturing, University of Tennessee, Knoxville, Tennessee 37996, USA*

The low-energy properties of transition metal oxides (TMOs) are governed by the electrons occupying strongly correlated d-orbitals that are hybridized with surrounding ligand oxygen p orbitals to varying degrees. Their physics is thus established by a complex interplay between the transition-metal (TM)-ligand hopping t, charge transfer energy Δ_{CT}, and on-site TM Hubbard repulsion U. Here, we study the spectral properties of a one-dimensional (1D) analog of such a pd system, with alternating TM d and ligand anion p orbitals situated along a chain. Using the density matrix renormalization group method, we study the model's single-particle spectral function, x-ray absorption spectrum, and dynamical spin structure factor as a function of Δ_{CT} and U. In particular, we present results spanning from the Mott insulating ($\Delta_{\mathrm{CT}} > U$) to negative charge transfer regime $\Delta_{\mathrm{CT}} < 0$ to better understand the ground and momentum-resolved excited state properties of these different regimes. Our results can guide new studies on TMOs that seek to situate them within the Mott-Hubbard/charge transfer insulator classification scheme.

I. INTRODUCTION

Transition metal oxides (TMOs) are a broad class of quantum materials that have long held the attention of materials scientists and condensed matter physicists [1–5]. These materials host transition metal cations surrounded by oxygen anions and exhibit a rich set of electronic, magnetic, optical, and structural properties that can be tuned through subtle changes in different tuning parameters (e.g., strain, composition, temperature, pressure, etc.). As such, they have the potential to advance many technologies in energy storage, sensing, catalysis, spintronics, and beyond [6–10].

The low-energy electronic structure of TMOs and, consequently, their functional properties are determined by their partially filled transition metal (TM) $3d$ orbitals, which are often hybridized to the $2p$ orbitals of the surrounding oxygen ligands. A unifying organizational principle behind these materials is the Zaanen-Sawatzky-Allen (ZSA) scheme [5], which classifies each material based on the relative values of the charge-transfer (CT) energy Δ_{CT} and interatomic TM Hubbard repulsion U. Defined in the atomic limit, U characterizes the energy associated with $d_i^n d_{i+1}^n \rightarrow d_i^{n-1} d_{i+1}^{n+1}$ charge excitations between the TM cations, where d_i^n denotes the valance state of the cation at site i. Conversely, Δ_{CT} is the energy associated with transferring a hole from the TM site to the surrounding ligand orbitals, i.e., $d_i^n \rightarrow d_i^{n+1}\underline{L}$, where $\underline{L}$ denotes a ligand hole. If $U > \Delta_{\mathrm{CT}}$, charge transfer to the ligand sites is the primary barrier to transport, and the system is a charge-transfer insulator (CTI). Conversely, if $U < \Delta_{\mathrm{CT}}$, Hubbard-like excitations between the TM sites limit transport, and the system is a Mott-Hubbard insulator. If $U \approx \Delta_{\mathrm{CT}}$, then the system is said to be of a mixed character. There also exists so-called negative charge-transfer insulators (NCTIs), where $\Delta_{\mathrm{CT}} < 0$ such that holes self-dope onto the ligand orbitals [11, 12]. Correlated materials with cations in high oxidation states often fall into this latter category [12–16].

Properly classifying a material has important implications for understanding its functional properties. For example, the quasi-1D and 2D cuprates are CTIs, which helps account for their large superexchange interactions and robust antiferromagnetism [17–21]. Similarly, the recent discovery of superconductivity in the low-valence nickelates [22–25] launched a significant effort [26–38] aimed at classifying these materials. Understanding the fundamental differences between nickel and copper oxides can illuminate the basic ingredients for high-T_{c} superconductivity. Similarly, several classes of NCTIs have been identified with strong coupling to TM-O bond-stretching phonon modes [39–42] that arises directly from the strong hybridization between the ligand and TM states. This interaction has been proposed as the mechanism behind charge ordered phases [39, 40, 42], bipolaronic transport [43, 44], and high-T_{c} superconductivity [45–47].

Given the diverse physics realized by variations in Δ_{CT} and U, it is important to develop spectroscopic methods for determining which regime a material occupies. Significant progress has been made in understanding the fundamental properties of TMOs through the use of small cluster exact diagonalization calculations in the context of core-level spectroscopies [11–14, 21, 28, 48–55]. These include calculations incorporating all five d orbitals and effective three-band models (one $d_{x^2-y^2}$ and two p bands) using exact diagonalization (ED) [56–58]. However, scaling these many-body calculations to extended clusters needed for calculating other dynamical properties has been challenging. For example, sophisticated numerical approaches such as the density matrix renormalization group (DMRG) have only recently been applied to studying the excitation spectra of corner-shared CuO_3 chains [59, 60] and ladders [61]. The fermion sign problem limits quantum Monte Carlo calculations [62–65], while cluster sizes can limit quantum embedding techniques [66–68].

The complexity of the underlying problem is such that

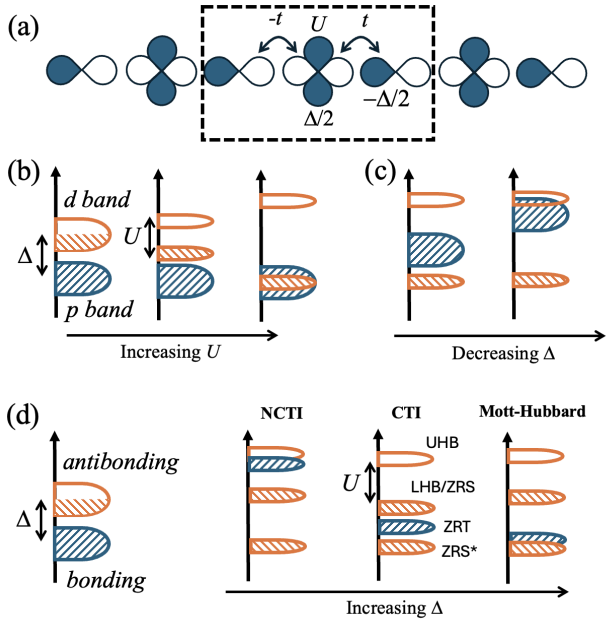

FIG. 1. (a) Cartoon of the Cu-O chain studied in this work, described by a two-band Emery Hamiltonian, see Eqs. (1)-(3). In our calculation, we use a similar geometry, with L unit cells and an extra oxygen, as shown here for $L = 3$. (b), (c) Illustration of the density of states for the atomic picture ignoring hybridization effects between the bands (see text), with p and d states separated by an energy splitting Δ. Shading represents different occupied states. Panels in (b) show the effect of introducing a Coulomb repulsion U on the d orbitals for positive Δ. This regime corresponds to a Mott-Hubbard insulator. The effects of decreasing Δ are depicted in (c). Finally, panel (d) shows both hybridization and many-body effects, and illustrates the crossover from negative charge transfer insulator to Mott-Hubbard insulator as Δ varies from negative to positive, shifting the relative center of mass of the bands.

one needs to resort to effective low-energy theories with fewer degrees of freedom. While the single band Hubbard or t-J models may contain the fundamental ingredients to explain high-T_c superconductivity [2, 69–73], these mappings rely on two main assumptions: (i) that the the fundamental physics takes place in CuO_2 (or NiO_2) planes, and (ii) the Zhang-Rice singlet (ZRS) construction holds for describing the charge carriers in doped CTIs [74–81]. However, the validity of the ZRS picture is subject to the relative position of the d and p orbitals and remains controversial in systems with large CT energies [28, 82–86]. Moreover, the mapping onto an effective single band Hamiltonian assumes that higher-energy charge transfer states can be ignored, which is not all obvious when Δ_{CT} is small or negative. Optical conductivity experiments [87] in Zn-LSCO, for example, reveal a mixture of states with singlet and triplet characters that can only be explained using a multi-band model.

Motivated by these considerations, here we present a systematic study of the excitation spectra of simplified multi-orbital charge-transfer chains using the DMRG method. By focusing on a one-dimensional (1D) geometry, we can calculate the model's excitation spectra with high momentum resolution and explore a wide regime of parameters. Albeit 1D, our model contains the basic ingredients needed to study the crossover between different regimes of the ZSA classification scheme, with carriers that can be defined in terms analogous to the ZRS in higher dimensions [88]. By focusing on a 1D model we can also make direct connections with a large body of existing literature. For example, undoped 1D cuprates such as Sr_2CuO_3 and $SrCuO_2$ have been widely studied using a variety of experimental probes [32, 89–102] while angle-resolved photoemission spectroscopy (ARPES) [103] and resonant inelastic x-ray scattering (RIXS) [104] experiments have recently been carried out on the related doped compound $Ba_{2-x}Sr_xCuO_{3+\delta}$. This family of materials has been analyzed using both multi-orbital models and effective single-band Hamiltonians [59, 103–109]. For simplicity, here we focus on a two-band model alternating TM and O orbitals along the chain. Despite its apparent simplicity, this model exhibits rich physics as a function of the band splitting, hopping, and interaction strengths.

The manuscript is organized as follows: Section II introduces our model and outlines the details of our DMRG calculations. Section III then presents results, including predictions of the single-particle spectral function (Sec. III B), x-ray absorption spectroscopy (XAS) (Sec. III C), and dynamical spin structure factor (Sec. III D). In each case, we are particularly interested in tracking the evolution of various spectral features as a function of the Hubbard interaction U and CT energy Δ_{CT}. Finally, Sec. IV discusses our results and summarizes our findings.

II. MODEL AND METHODS

A. Model: the one-dimensional pd-chain

We consider a two-band model with alternating $3d_{x^2-y^2}$ and $2p$ orbitals along a 1D chain [88, 110], as shown in Fig. 1a. The unit cell contains one p and one d orbital, while the index i indicates the position of the d orbital along the chain. The model's Hamiltonian, written in electron language, is

$$H = H_0 + H_U. \tag{1}$$

Here,

$$H_0 = -t \sum_{i,\sigma,\delta} P_\delta \left(d^\dagger_{i,\sigma} p_{i+\delta,\sigma} + \text{H.c.} \right) + \frac{\Delta}{2} \sum_{i,\sigma,\delta} (n^d_i - n^p_i), \tag{2}$$

includes the noninteracting terms and

$$H_U = U \sum_i n^d_{i,\uparrow} n^d_{i,\downarrow} \tag{3}$$

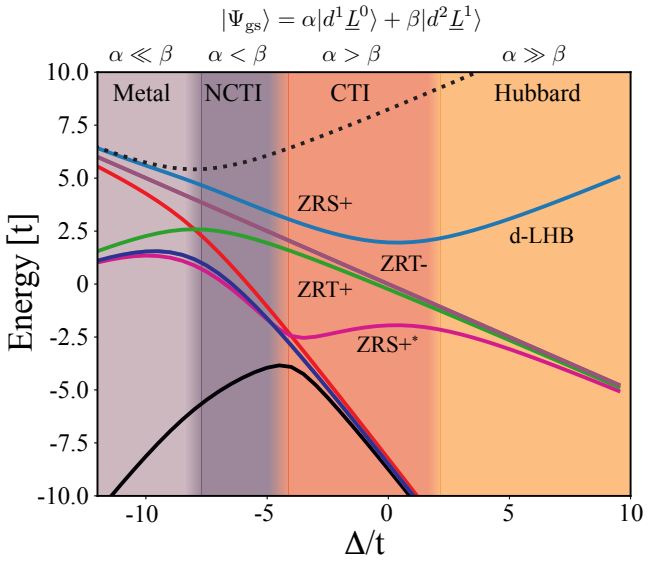

FIG. 2. The electron addition and removal spectrum of a three site p-d-p cluster, as shown in the dashed box of Fig. 1. The energies were obtained by exact diagonalization with $U = 8t$. The full (dashed) lines correspond to the single-particle removal (addition) states. Vertical dash lines correspond to $\Delta = -8$ ($\Delta_{\rm CT} = 0$) and $\Delta = 0$ ($\Delta_{\rm CT} = U$), which correspond to the approximate positions of the crossovers between the different regimes. The labels above each region indicate the dominant character of the one-hole ground state.

is the on-site Hubbard interaction for the d orbitals. In these expressions, the fermionic operators $d^\dagger_{i,\sigma}$ ($d_{i,\sigma}$) and $p^\dagger_{i,\sigma}$ ($p_{i,\sigma}$) create (annihilate) a spin σ ($=\uparrow,\downarrow$) electron on the $3d_{x^2-y^2}$ and $2p$ orbitals in unit cell i, respectively, $n^{p/d}$ is the corresponding number operator, $i+\delta = i \pm 1$ indicates the p orbitals situated on either side of the d orbitals, and $P_{\delta=\pm} = \mp 1$ is a phase factor for the pd hopping.[1] The on-site Coulomb interaction for the d orbitals is U and the nearest-neighbor pd hopping $t = 1$ sets our unit of energy.

Throughout this work, we follow the ZSA [5] scheme for describing the system, which starts from the atomic limit ($t = 0$).[2] Using our definition of the Hamiltonian, the d levels will split into states centered at $\Delta/2$ and $\Delta/2 + U$, while the p levels are centered at $-\Delta/2$. The CT energy $\Delta_{\rm CT}$ is equal to the energy difference between the $d^2\underline{L}^1$ and $d^1\underline{L}^0$ configurations in the atomic limit and thus given by $\Delta_{\rm CT} = \epsilon_d - \epsilon_p + U = \Delta + U$. Once we reintroduce the electron hopping, these states form bands and acquire a finite bandwidth W, as sketched in Figs. 1(b)-(f). Finally, which we fix to $U = 8t$ unless stated otherwise and vary Δ to control the charge transfer energy. For reference, typical values for these parameters in cuprate materials are $t \approx 250 - 500$ meV, $U \approx 8 - 12$ eV, and $\Delta \approx 2 - 4$ eV depending on the material [59, 66, 89, 111–115].

Even though the ZSA picture provides some intuition for the electronic structure, it misses a few important aspects about the effects of the lattice and the hybridization between orbitals. To see this, one can instead start from the noninteracting limit, where the orbitals form bonding (-) and antibonding (+) bands with dispersion

$$\epsilon_\pm(k) = \pm\sqrt{4t^2\sin^2(ka/2) + \Delta^2/4}, \tag{4}$$

where a is the lattice constant.[3] For large $\Delta > t$, the antibonding band has mostly d character and, in the presence of interactions, it will split into a lower Hubbard band (LHB) and an upper Hubbard band (UHB) [116]. The system is classified as a Mott-Hubbard insulator when the chemical potential lies between the two Hubbard bands. When $\Delta \lessapprox t$, the system is in a regime of strong hybridization, and for negative Δ, but small compared to U, the system becomes a CTI. Finally, for large negative Δ, the system enters a NCTI regime [11] in which the antibonding band has mostly p character, and the system can become metallic (or "self-doped") by mixing with the UHB.

B. Methods

We calculate the model's spectral functions using the time-dependent density-matrix renormalization group (tDRMG) [117–120]. Specifically, we compute the single particle two-time correlator

$$G_{d/p}(x,t) = \mathrm{i}\langle O^\dagger_\sigma(i,t) O_\sigma(L/2,0)\rangle, \tag{5}$$

where the operator $O^\dagger_\sigma(i,t) = d^\dagger_{i,\sigma}(t)$ or $p^\dagger_{i,\sigma}(t)$ defines the character of the excitation. This quantity is Fourier transformed to frequency and momentum, yielding the spectral function $A_{d/p}(k,\omega) = -\mathrm{Im}G_{p/d}(k,\omega)/\pi$. Similar expressions are used to compute the dynamical spin structure factor $S^z(k,\omega)$, where the spin operator $O = S^z_{p/d}$ is used instead. We can also calculate the XAS spectra using a similar approach but with a modified Hamiltonian that accounts for the core hole's interaction with the valence electrons (see Sec. III C) [121].

[1] The sign in the hopping can be removed with a simple gauge transformation [88]. However, we keep it in place to avoid artificial phases in the momentum-resolved correlation functions.

[2] To reconcile our model with ZSA's, notice that they set $\epsilon_d = 0$ and $\epsilon_p = \Delta$ so there is a downward shift of the energy levels by $-\Delta/2$ in our case.

[3] Analogs to these bands also appear in the 4-band model studied in Ref. 59 for corner-shared Cu-O chains, which also contains a nonbonding and a flat band that does not contribute to the physics of the system. Therefore, despite the apparent simplicity of our Hamiltonian, we expect it to realize many features relevant to real materials.

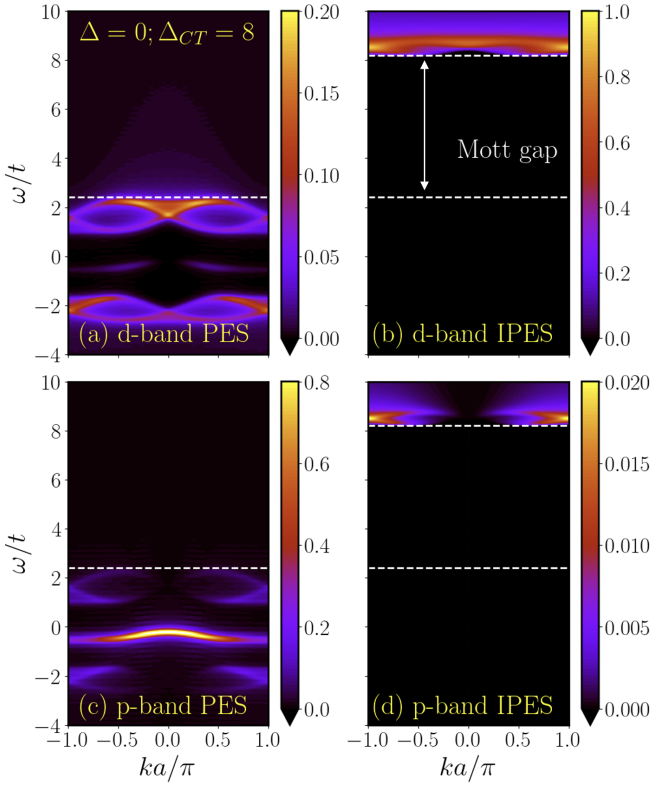

FIG. 3. Photoemission (electron removal –PES) and inverse photoemission (electron addition – IPES) spectra for the ligand (a);(b) d orbitals and (c);(d) p orbitals for fixed $U = 8t$. The density is fixed at $N_e = 3L + 2$, where $L = 64$ is the number of unit cells

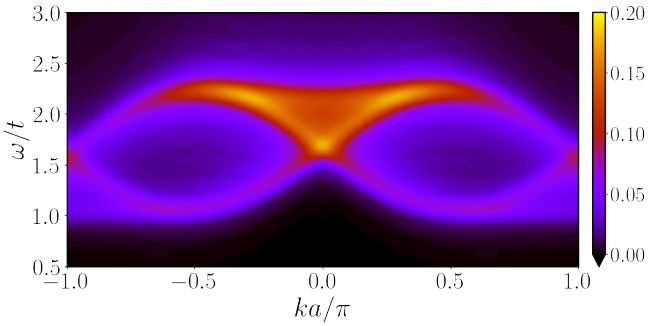

FIG. 4. Photoemission (electron removal – PES) spectrum for the d orbitals. Same data as in Fig.3(a) but zooming-in onto the lower Hubbard band. The spectrum shows clear signatures of 1D physics, with spinon and holon bands.

We carried out all calculations on a chain with open boundary conditions and an extra oxygen p orbital on the left side of the chain. The total number of orbitals is $2L + 1$, where L is the number of unit cells. This cluster geometry preserves the reflection symmetry of the lattice with respect to the d orbital located at the center of the chain $i = L/2$. To reduce artifacts from Fourier transforming in a finite time window, we used a "Hann window" technique, convoluting the results with an exponential function that yields a Lorentzian lineshape with a width $\epsilon = 0.1$ [122]. This practice also helps mitigate errors that tend to accumulate at longer times. We typically use $m = 400$ DMRG states (guaranteeing a truncation error below 10^{-6}), a time step $\delta t = 0.02$, and a maximum time $\sigma = t_{\max} = 40$. The undoped (i.e., "half-filled" in the cuprate literature) stoichiometric case corresponds to three electrons per unit cell, two for each p orbital and one for each d, translating into a total of $N_e = 3L + 2$ electrons. Finally, we performed all simulations using a third-order Suzuki-trotter decomposition of the time evolution operator.

III. RESULTS

A. Ground State Properties

Before discussing our model's spectral properties, it is helpful to examine its ground state character as a function of model parameters. To this end, we carry out small cluster ED calculations, considering only two p orbitals and one d orbital in a p-d-p geometry, as sketched in the dashed box of Fig. 1(a).

We first solve this cluster for the stoichiometric filling with $N = 5$ electrons. The cluster's ground state in this sector can be written as a linear combination $|\Psi_{\rm gs}\rangle = \alpha\,|d^1\underline{L}^0\rangle + \beta\,|d^2\underline{L}^1\rangle$, where

$$\begin{aligned} |d^1\underline{L}^0\rangle &= |2,\uparrow,2\rangle\,, \\ |d^2\underline{L}^1\rangle &= \tfrac{1}{\sqrt{2}}\left[|\uparrow,2,2\rangle - |2,2,\uparrow\rangle\right]. \end{aligned} \tag{6}$$

Here, each number/spin denotes the occupation of the orbitals, d^n indicates n electrons in the d orbital, and $\underline{L}^n$ denotes n holes occupying the surrounding ligand oxygen orbitals (see also App. A).

Adding an electron produces a filled cluster described by the eigenstate $|d^2\underline{L}^0\rangle = |2,2,2\rangle$. Conversely, the eigenstates of two-hole cluster in the $S^z_{\rm tot} = 0$ sector are spanned by the basis

$$\begin{aligned} |d^0\underline{\rm L}^0\rangle &= |2,0,2\rangle\,, \\ |\overline{2\uparrow\downarrow}\pm\rangle &= \tfrac{1}{\sqrt{2}}\left[|2,\uparrow,\downarrow\rangle \mp |\downarrow,\uparrow,2\rangle\right], \\ |\overline{2\downarrow\uparrow}\pm\rangle &= \tfrac{1}{\sqrt{2}}\left[|2,\downarrow,\uparrow\rangle \mp |\uparrow,\downarrow,2\rangle\right], \\ |\overline{\downarrow 2\uparrow}\pm\rangle &= \tfrac{1}{\sqrt{2}}\left[|\downarrow,2,\uparrow\rangle \pm |\uparrow,2,\downarrow\rangle\right], \text{ and} \\ |\overline{220}\pm\rangle &= \tfrac{1}{\sqrt{2}}\left[|2,2,0\rangle \pm |0,2,2\rangle\right]. \end{aligned} \tag{7}$$

The states $|\overline{2\uparrow\downarrow}\pm\rangle$ and $|\overline{2\downarrow\uparrow}\pm\rangle$ are related by time reversal symmetry. The Hamiltonians in the symmetric and antisymmetric channels are 5×5 and 4×4 matrices (their explicit form is given in App. A), which can be diagonalized numerically. The excited state spectrum

is shown in Fig. 2 for $U = 8t$. Here, the electron removal spectrum is obtained from the energy difference $E_0(5) - E_n(4)$ while the electron addition spectrum is obtained from $E_n(6) - E_0(5)$, where $E_n(N_e)$ denotes the eigenenergy of the cluster with N_e electrons.

The two-hole eigenstates in the $S^z_{\rm tot} = 0$ sector can be written in a general form

$$|\Psi\rangle = \alpha\,|d^0\underline{\rm L}^0\rangle + \tfrac{\beta}{\sqrt{2}}\left[|\overline{2\uparrow\downarrow}\pm\rangle \pm |\overline{2\downarrow\uparrow}\pm\rangle\right] + \delta\,|\overline{\downarrow\,2\uparrow}\pm\rangle + \gamma\,|\overline{220}\pm\rangle\,. \tag{8}$$

The state equivalent to the ZRS in this model is

$$|{\rm ZRS}+\rangle = \alpha\,|d^0\underline{\rm L}^0\rangle + \tfrac{\beta}{\sqrt{2}}\left[|\overline{2\uparrow\downarrow}+\rangle - |\overline{2\downarrow\uparrow}+\rangle\right], \tag{9}$$

which is symmetric under reflections about the d orbital. Notice that the additional hole is pure of p (d) character if α (β) is zero but has mixed character in general. We can also define a state similar to the ZRS but using the antibonding combination of the p-states hybridized with the d orbital

$$|{\rm ZRS}+^*\rangle = \beta\,|d^0\underline{\rm L}^0\rangle - \tfrac{\alpha}{\sqrt{2}}\left[|\overline{2\uparrow\downarrow}+\rangle - |\overline{2\downarrow\uparrow}+\rangle\right]. \tag{10}$$

These two states undergo an avoided level crossing at $\Delta \sim 0$ ($\Delta_{\rm CT} = U$). In addition to the ZRS excitations, we can define an antisymmetric counterpart $|{\rm ZRS}-\rangle$ that does not include the $|d^0\underline{\rm L}^0\rangle$ state, as well as Zhang-Rice triplets $|{\rm ZRT}\pm\rangle$ with the added hole completely localized in the p orbital.

Figure 2 shows results for the cluster's electron addition and removal eigenstate spectrum for $U = 8t$. The vertical dashed lines indicate the approximate transitions between the Mott-Hubbard, CTI, and NCTI regimes. (Note: the locations of these divisions are a bit arbitrary since they denote crossover points rather than phase transitions.) The labels on the top of each region highlight the dominant character of the half-filled cluster's ground state. The dashed curve follows the energy of the $|d^2\underline{L}^0\rangle$ state, which we associate with the upper Hubbard band. In the Mott-Hubbard regime ($\Delta > 0$, $\Delta_{\rm CT} > U$), the additional doped hole has predominantly d character. Conversely, in the CTI regime ($0 > \Delta > -U$, $U > \Delta_{\rm CT} > 0$), the doped hole has predominantly p character. In the NCTI regime ($\Delta < -U$, $\Delta_{\rm CT} < 0$), the lowest energy states will develop important additional weight in the states involving a double occupied d orbital and two p holes, i.e. $|\overline{220}+\rangle$ and $|\overline{\downarrow\,2\uparrow}+\rangle$ [12]. The lowest energy hole excitation, which we associate with the highest energy state in Fig. 2, is $|{\rm ZRS}+\rangle$. It is followed by the $|{\rm ZRS}-\rangle$ state, the Zhang-Rice triplets $|{\rm ZRT}\pm\rangle$, and the antibonding $|{\rm ZRS}+*\rangle$ states. The lower band can be associated with excitations with dominant d characters.

When contrasting with the ZSA picture, we first notice that the lower d band splits into symmetric and antisymmetric bands. One usually projects out the antisymmetric band in the Zhang-Rice treatment of the problem since they are high energy states [74]. The symmetric band can be associated with the ZRS band in the multiorbital problem, and it always appears above the triplet p band. The most relevant parameter to characterize the problem is the splitting between the triplet p states and the ZRS band, which gets smaller as Δ becomes more and more negative. When $\Delta \lesssim -U$, the system enters the NCTI regime, and the triplet p, ZRS, and UHB states all mix, and the system becomes metallic.

B. Electron addition and removal spectra

Having examined a simplified energy level diagram for our model, we now turn our attention to the electron addition and removal spectra, focusing first on the case with $U = 8t$ and $\Delta = 0$ ($\Delta_{\rm CT} = 8t$), as shown in Fig. 3. This case corresponds to the strongly covalent or mixed Mott-Hubbard/CTI regime. We remind the reader that we use electron language in the following discussion, so the UHB (LHB) corresponds to states with two (zero) electrons occupying a d orbital.

In the half-filled, noninteracting case, the system's electronic structure consists of bonding and antibonding pd bands [see Eq. (4)] with the Fermi level located in the center of the antibonding states. Introducing a large U redistributes the spectral weight into Hubbard and Zhang-Rice bands. The UHB is apparent in the electron addition spectra, appearing in Figs. 3(b) and (d) as a band of states centered at $\omega \approx U$. In this case, the UHB's spectral weight has a majority d character with a small admixture of p character. [Note the color bar scale change in panel (d).] We can also resolve three additional bands below the Fermi level. The highest and lowest-lying bands are the Zhang-Rice singlet states derived from the bonding and antibonding ZRS states $|{\rm ZRS}+\rangle$ and $|{\rm ZRS}+*\rangle$, respectively. These states have majority d character at $k = 0$ but acquire p character at the zone boundary. This weight reflects the fact that one cannot construct long wavelength Bloch states using the molecular p orbitals of the form $L^\dagger = \frac{1}{\sqrt{2}}[p^\dagger_{i+1,\sigma} - p^\dagger_{i-1,\sigma}]$. The narrow band of states appearing just below $\omega = 0$ is derived from the Zhang-Rice triplet states; it has majority p character because the $|{\rm ZRT}\pm\rangle$ state places the additional hole entirely on the p orbitals.

Due to the 1D geometry, our interacting system cannot be adiabatically connected to a Fermi liquid. Thus, many of the bands display clear signatures of spin-charge separation, with spinon branches in the d bands that form an arc between $\pm k_{\rm F}$ and wider holon bands corresponding to the charge excitations [88, 109, 123–125]. As illustration, we zoom in on Fig. 3 to show the holon and spinon branches in the LHB. The behavior observed in Fig.4 is typical of 1D TM oxides, such as $Ba_{2-x}Sr_xCuO_{3+\delta}$[103]. Moreover, this also indicates that the spin is mostly localized in the Cu d orbitals. Moreover, this also indicates that the spin is mostly localized in the Cu d orbitals. The bandwidth of the UHB is smaller than the bandwidth of the ZRS-derived states because electrons have

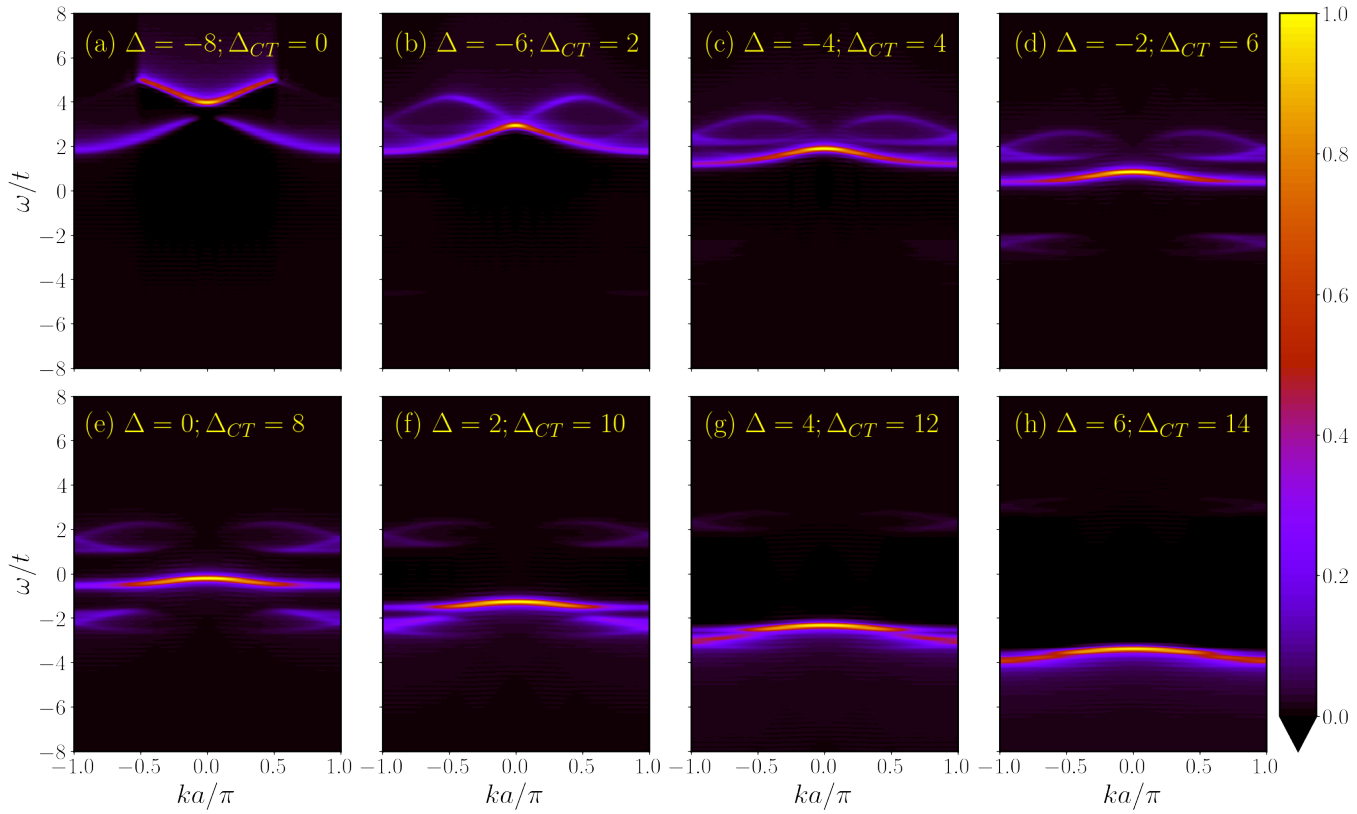

FIG. 5. Photoemission (electron removal) spectra for the ligand p orbitals for $U = 8t$ as the system crosses from the Mott-Hubbard regime to the CTI and NCTI regimes for decreasing energy splitting Δ. The density is fixed at $N_e = 3L + 2$, where $L = 64$ is the number of unit cells (see text).

to hop over the p-d-p bridge to propagate, a higher order process involving the virtual double occupation of a d orbital (the effective hopping is of the order $t^2/(U - \Delta)$ [88]). Notice that the three- or four-band models studied previously include p-p hopping processes that allow electrons to bypass the d orbital.

Next, we vary the degree of the hybridization by adjusting Δ. Figs. 5 and 6 plot results for the electron removal (photoemission spectrum) as a function of Δ while again fixing $U = 8t$. With increasing $\Delta > 0$, the splitting between bonding $|\mathrm{ZRS}+\rangle$ and antibonding $|\mathrm{ZRS}+*\rangle$ bands increases while the $|\mathrm{ZRT}\pm\rangle$ band moves downward in energy. For $\Delta = 6t$ ($\Delta_{\mathrm{CT}} = 14t$), the system is in the Mott insulating regime and two bands strongly overlap, while the d spectral weight is mainly concentrated on the antibonding state at high energy (see Fig. 6). In this regime, one can project out the p degrees of freedom in the low-energy sector to obtain an effective single-band Hubbard Hamiltonian [5, 110]. For $-U < \Delta < 0$ ($0 < \Delta_{\mathrm{CT}} < U$), the system is in the CTI regime. In this case, the $|\mathrm{ZRT}\rangle$ states moves upward in energy with decreasing Δ and eventually overlap with the antibonding $|\mathrm{ZRS}+*\rangle$ states. Between $\Delta = -6t$ and $\Delta = -8t$, Zhang-Rice and UHB states all mix, and the system becomes metallic [49].

C. XAS

Next, we examine the XAS spectra for our model to make contact with prior small cluster calculations. XAS is a single photon process in which an electron is excited from a core orbital into an empty or partially filled valence orbital [126, 127]. It thus probes the system's unoccupied density states but with corrections introduced by the interaction between the valence electrons and the core hole created by the absorption process. These corrections can sometimes be strong since the electrons will try to screen the core hole and form a bound state [126–128].

We calculate the XAS spectra using the time-dependent formalism described in Ref. 121. In this case, the spectrum is obtained from the imaginary part of the Fourier transform of a single-particle time-dependent correlation function $\langle c_0 \exp(-\mathrm{i}\mathcal{H}_c t) c_0^\dagger \rangle$, where the operators act on a reference site $i = 0$, which could be either a p or d orbital, depending on the absorption edge that is used in the experiment [126, 127]. The Hamiltonian $\mathcal{H}_c$ in this expression includes the interaction between the core-hole and the valence band electrons. Assuming that the core hole is immobile, we model this interaction using

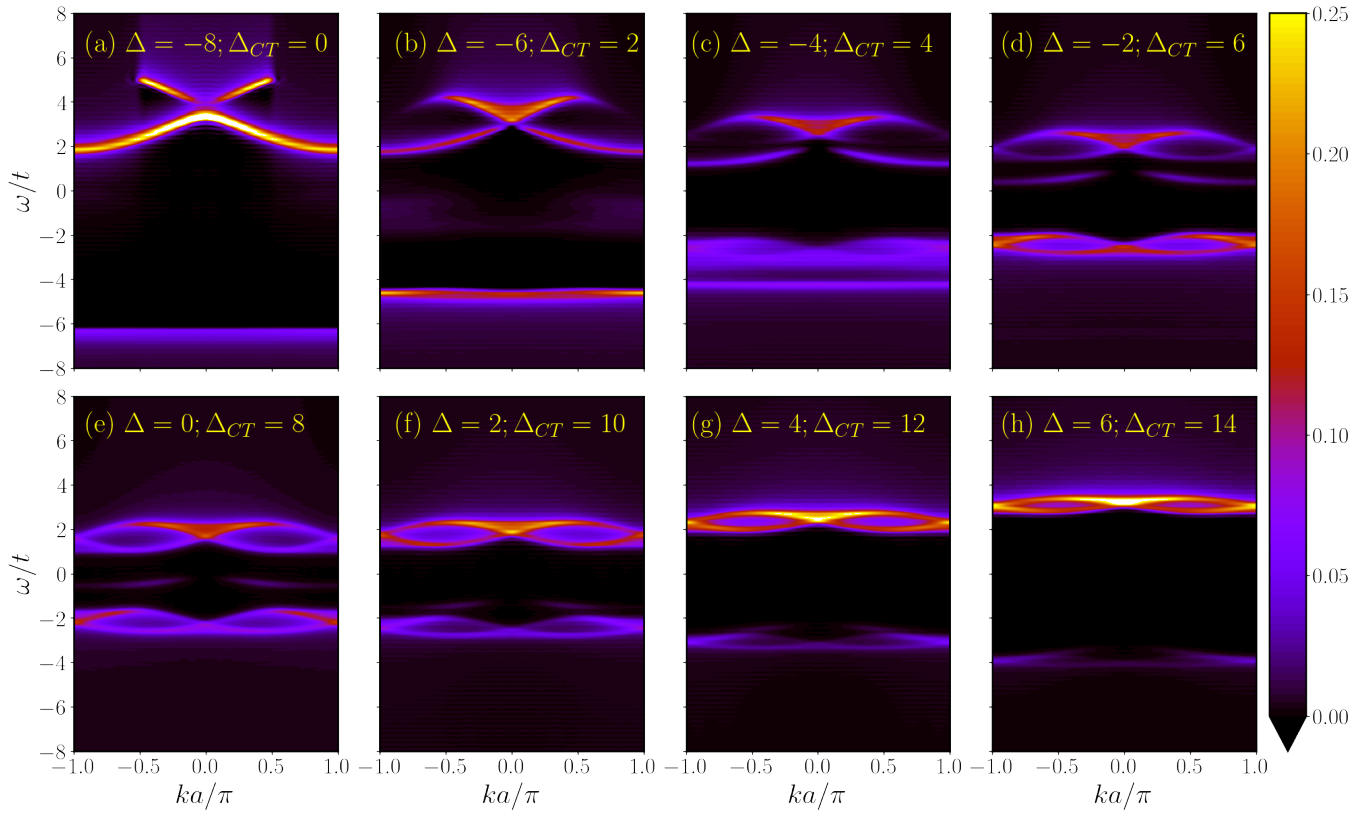

FIG. 6. Same as Fig. 5 but for the d orbitals.

an on-site atomic potential such that

$$\mathcal{H}_c = H + U_c \sum_\sigma c^\dagger_{0,\sigma} c_{0,\sigma}, \tag{11}$$

where H is the original two-band Hamiltonian given in Eqs. (1)-(3) and U_c is the attractive potential created by the core hole. The rest of the calculation steps are identical to those used for the photoemission spectrum. We refer the reader to Ref [121] for further details.

To focus on results that can help intuitively interpret experiments conducted on doped cuprate chains, we consider $L = 16$ and $N_e = 44$, corresponding to a slightly hole-doped case. The XAS spectra for fixed $U = 8t$ are shown in Fig. 7 for several values of Δ. Here, we present results for both K-edge (p) and L-edge (d) experiments. In call cases, we fixed the core-hole potential to $U_c = -1.5t$.

For a large positive $\Delta = 6t$ [$\Delta_{\rm CT} = 14t > U$, see Fig. 7(h)], the doped holes predominantly reside in the lower Hubbard d band while the p orbitals are nearly completely filled. This charge distribution Pauli blocks the core electron from being excited into the p orbital, and the resulting K-edge spectrum is dramatically suppressed as a result. Instead, a core electron can be excited into an unoccupied d orbital at the L-edge. In the doped system, these transitions can occur to an empty d orbital or a half-filled one with the opposite spin orientation. The corresponding XAS spectra thus consist of two resonances corresponding to the two possible final state configurations, which appear at $\omega \approx \Delta/2 + U_c$ and $\Delta/2 + U + 2U_c$. In this regime, the system behaves qualitatively similar to the atomic limit.

The XAS spectra preserve these features as Δ decreases, until crossing into the CTI regime for $\Delta \leq 0$ ($\Delta_{\rm CT} \leq U$). The p and d states become strongly hybridized in this regime, and the spectra develop new features. The first is the secondary peak in the d spectrum at energy $\sim \Delta/2 + U + U_c$, which corresponds to the "poor-screened" resonance in which the core electron is excited into a delocalized state, leaving the d orbital at the site where the core hole is created half-filled. The second is the increased intensity of the p resonance, which eventually merges with the lower p resonance at sufficiently small Δ. These results show that the doped holes have predominant d character in the Mott-Hubbard regime, while they acquire a mixed d-p character in the CTI regime. We can thus associate the lower d resonance to the Zhang-Rice state in the latter case.

D. Spin excitations

Finally, we examine the model's spin excitations. This analysis is motivated by efforts to understand the so-called missing spectral weight problem in neutron

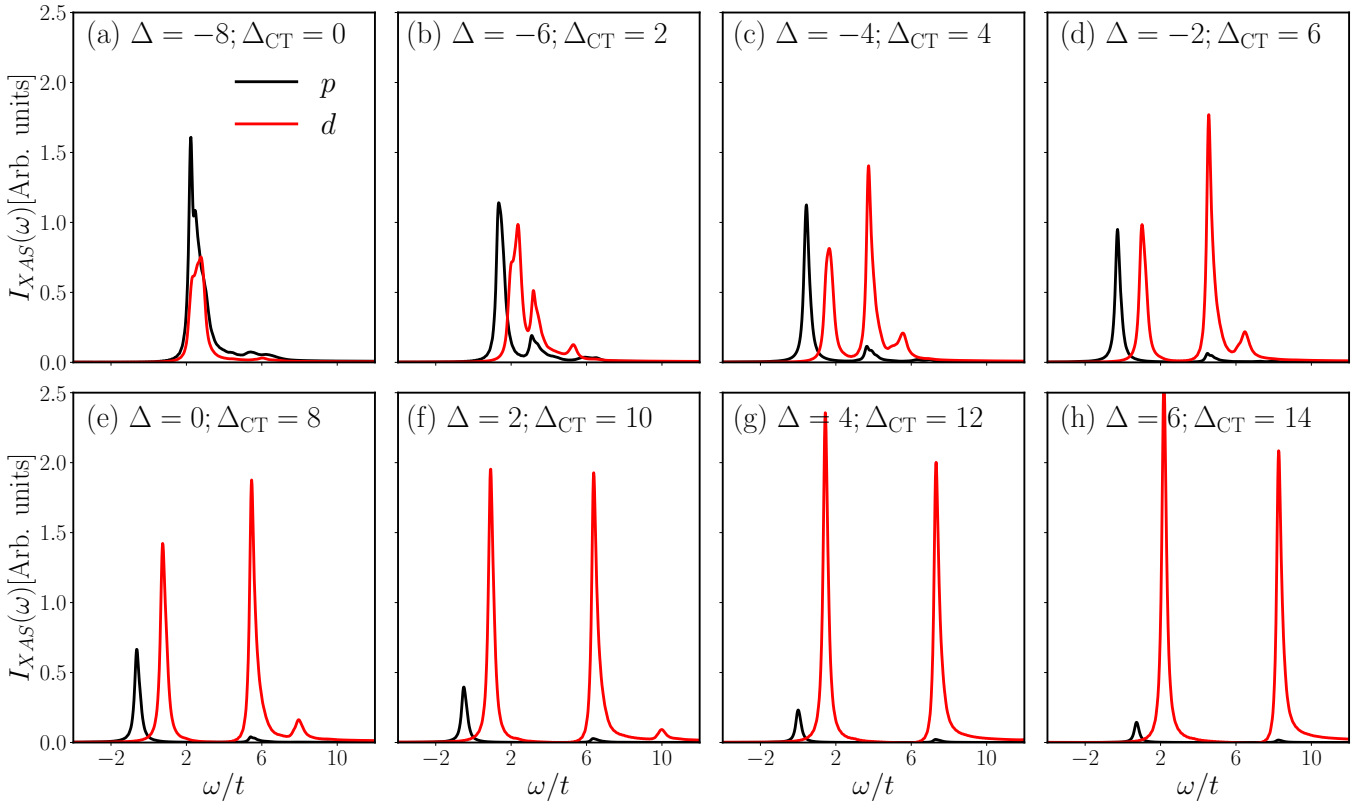

FIG. 7. XAS spectra of an Emery chain for different values of Δ. The spectra were calculated for small hole doping ($L = 16$; $N_e = 44$), fixed $U = 8t$, and core-hole potential $U_c = -1.5t$.

scattering experiments conducted on low-dimensional cuprates [59, 93, 129–132].

The dynamical spin structure factor $S(q, \omega)$ obeys a sum rule relating its integrated spectral weight to the total magnetic moment in the unit cell. For a 1D system, can define the integrated spectral weight up to a cut-off ω_c

$$m(\omega_c) = \frac{3}{N} \sum_{\alpha,\beta,q} \int_0^{\infty} S^z_{\alpha,\beta}(q,\omega) e^{iq(r_\alpha - r_\beta)}, \qquad (12)$$

where α and β are orbital indices in the unit cell, r_α is the basis vector for the orbital, and $S^z_{\alpha,\beta}(q,\omega)$ is the dynamical spin structure factor. In the $\omega_c \to \infty$ limit, $m(\omega_c)$ should recover a value set by the total local moment in the unit cell. In particular, for our model

$$\lim_{\omega_c \to \infty} m(\omega_c) = \langle (S^z_d)^2 \rangle + \langle (S^z_p)^2 \rangle + 2\langle S^z_p S^z_d \rangle, \qquad (13)$$

where the expectation values are evaluated using the two-orbital unit cell. (In practice, we use the unit cell at the center of the chain.)

Early experiments on cuprate spin chains [93] and two-dimensional (2D) high-T_c superconducting cuprates [129–131] found that integrating the observed low-energy spectral weight ($\omega_c \lesssim 0.6$ eV) often recovered less than a third of the total expected weight for a Cu^{2+} ion, even after accounting for quantum fluctuations. It was later recognized that Cu-O hybridization effects play a key role here. For example, $\approx 80\%$ of the sum rule is recovered from inelastic neutron scattering (INS) measurements on Sr_2CuO_3 once the Cu-O form factor is taken into account [132]. A subsequent determinant quantum Monte Carlo (DQMC)/DMRG study of multi-orbital *pd*-model for the corner-shared cuprates [59] showed that remaining weight transfers to high-energy antibonding oxygen states. Notably, no such transfer occurs for similar simulations for the single-band Hubbard model [59].

Motivated by this, we now explore the evolution of the magnetic excitation spectrum and resulting deviations from the expected sum rule for our model as the degree of *p*-*d* hybridization varies. In general, the elementary magnetic excitations of our 1D chains are spinons. While the system may exhibit short-ranged or algebraically decaying spin-spin correlations, it cannot develop true long-range order and coherent magnon excitations. Since spinons are domain wall-like excitations, they are created in pairs when the system is probed with scattering techniques like INS or RIXS. Hence, the resulting magnetic excitation spectrum displays a continuum of two-spinon excitations, characteristic of 1D spin chains.

The present case adds a new ingredient: the charge-transfer energy Δ_{CT}. In our model, the spin-spin interactions are mediated by superexchange mechanisms

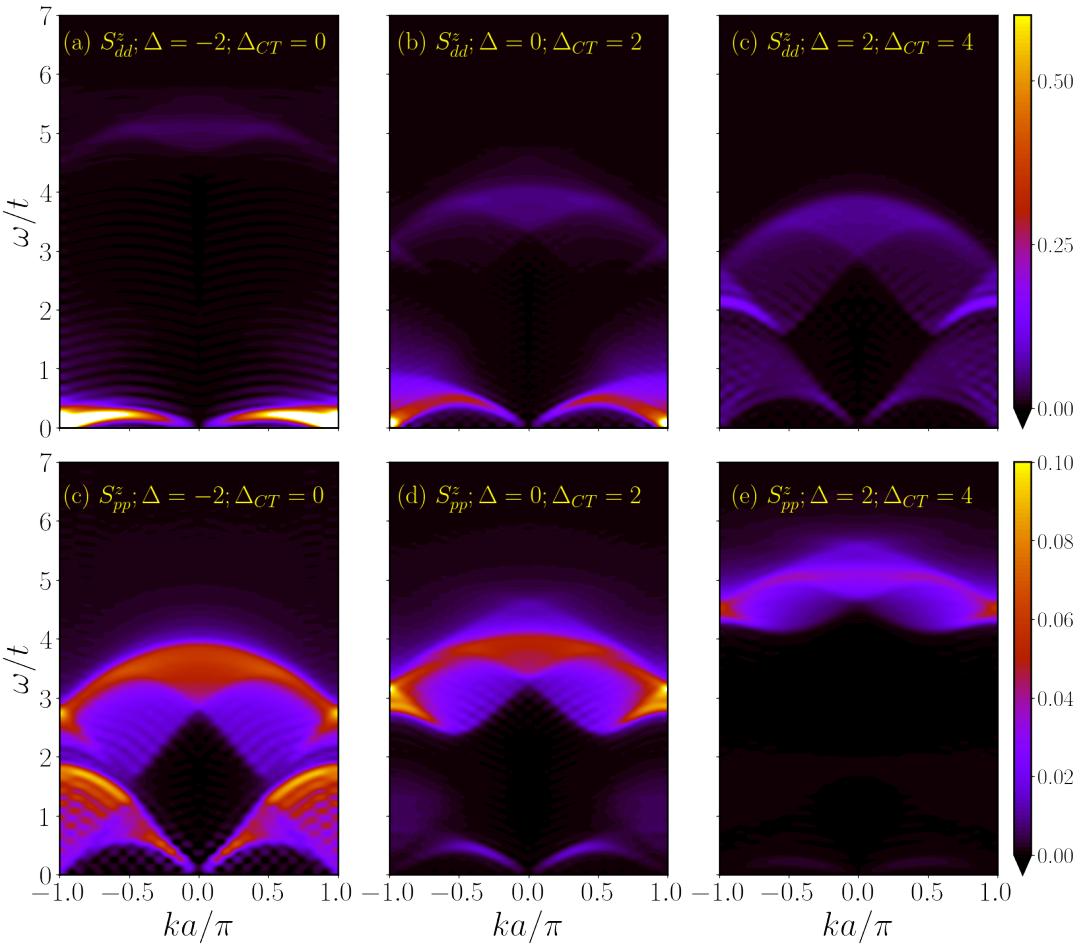

FIG. 8. Spin dynamic structure factor $S^z_{\alpha,\alpha}(k,\omega)$ obtained in $L = 32$ site half-filed chains with $U = 2t$ and different values of Δ as indicated in each panel. The top row shows the projection for the $\alpha = d$ orbitals, while the bottom row shows the projection for the $\alpha = p$ orbitals.

through the ligand p orbital and involve an intermediate process in which a p electron virtually double occupies a d state. This process is significantly suppressed for large $\Delta_{\rm CT}$ or U, resulting in a weak interaction between spins in this limit. For this reason, here we focus on a parameter regime with smaller $U = 2$ and Δ to study the spin excitations, which produces a reasonably large band width for the spinon excitations. Specifically, we calculate the orbital-resolved dynamic spin structure factors $S^z_{\alpha\beta}(q,\omega)$ for $\alpha = \beta = p, d$ on $L = 32$ chains.

The results for various values of Δ spanning from the strongly covalent ($\Delta = -2t$, $\Delta_{\rm CT} = 0$) to the mixed Mott/CTI ($\Delta = 0$, $\Delta_{\rm CT} = 2t = U$) to the Mott-Hubbard ($\Delta = 2t$, $\Delta_{\rm CT} = 4t > U$) regimes are shown in Fig. 8. In all cases, spin excitations are dominated by contributions from the d orbitals, consistent with most of the magnetic moment residing on those orbitals. We further observe a nonnegligible amount of spectral weight associated with the p orbitals, which is concentrated at higher energies. Varying the value of Δ affects the spectra in several notable ways. For example, increasing Δ increases the bandwidth of the excitations derived from the d states. It also transfers spectral weight from the low-energy d-derived excitations to the higher energy p-derived ones while causing the former to shift to lower energies. These effects are consistent with expectations for increased hybridization between the d and p orbitals.

Figure 9 further quantifies the redistribution of spectral weight of the magnetic excitations. Here the top row plots the momentum-integrated dynamical spin structure factor summed over all components $S^z(\omega) = \frac{1}{N}\sum_{\alpha,\beta,q} S^z_{\alpha\beta}(q,\omega)$, while the bottom panels show the corresponding $m(\omega_c)$ as a function of the energy cut-off. The red lines in the bottom panels indicate the average value of the moment squared, as obtained from Eq. (13). The results show that the total moment is distributed in energy, with some weight at very high energies. In particular, one must integrate to very high energy for $\Delta_{\rm CT} \geq U$ to recover the total expected sum rule. These results are consistent with a prior study that focused on the $\Delta > 0$ case [59], but derived here for different regimes of the ZSA classification scheme.

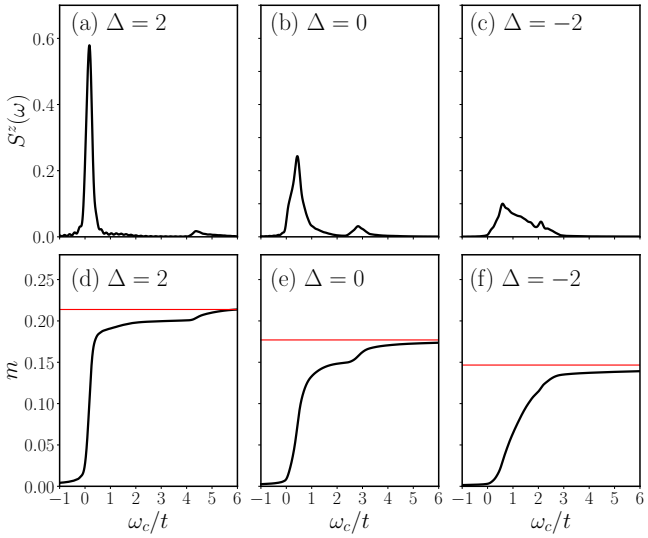

FIG. 9. (a)-(c) Momentum integrated spin dynamic structure factor $S^z(\omega)$ for $U = 2$ and different values of Δ. Panels (d)-(f) show the corresponding integrated spectral weight as a function of the cut-off frequency ω_c [see Eq. (12)]. The horizontal lines show the value of the local spin moment calculated directly using Eq. (13).

IV. SUMMARY & CONCLUSIONS

We have examined the ground and excited state properties of a 1D two-orbital model analogous to the *pd*-models used to describe charge-transfer TMOs. By focusing on a 1D system, we could calculate the model's excited state properties with high momentum resolution in different regimes of the ZSA classification scheme. In doing so, we provided predictions for the ground-state character, single-particle spectral function, XAS spectra, and dynamical spin structure factor for parameters spanning from the NCTI to CTI to Mott-Hubbard insulator regimes. Our results for the XAS spectra are broadly consistent with previous results obtained using small cluster methods [12, 14, 21, 133]. However, our results for the other dynamical correlation functions extend well beyond prior work focusing on a single parameter set [59] or previous mean-field treatments of the problem [40, 51].

One important aspect of our results is the predicted evolution of the magnetic sum rule. As mentioned in the introduction, considerable effort is often expended to situate newly discovered TMOs like the superconducting nickelates within the ZSA scheme. Based on our results shown in Fig. 9, we propose that the amount of missing local moment obtained from integrating the low-energy spin excitations could be used to quantify the degree of TM-O hybridization present in the material and infer the relative values of the charge-transfer energy and Hubbard interaction strength. INS measurements –corrected for the appropriate atomic form factor [99]– are ideally suited for such experiments. Analogous experiments with RIXS would be complicated by the fact that the measured spectra are not trivially related to $S(q, w)$ [134] with spectral weight that can be modified by other factors like electron-phonon coupling [135]. The predicted transfer of spectral weight to high-energy also has important implications for experimental attempts to measure entanglement witnesses like the quantum Fisher information, which often rely on particular sum rules [136, 137].

Moving forward, it would be interesting to dope our model and study how the canonical picture of anomalous spectral weight transfer in a doping a Mott insulator [133] changes as in the CTI and NCTI regimes. Such calculations can also be compared directly to data taken for the recently synthesized doped cuprate spin chains [103] and ladders [138, 139], where anomalous interactions have been inferred from comparing the observed spectra to effective singleband models.

DATA AND CODE AVAILABILITY

Data supporting this study is available on Zenodo[140]. Code is in the process of being made open-source through the ALPS package[141], and will be made available upon reasonable request.

ACKNOWLEDGMENTS

The authors acknowledge the support of the U.S. Department of Energy, Office of Basic Energy Sciences. This project was initiated under grant No. DE-SC0014407 and completed under grant No. DE-SC0022311. We thank A. A. Aligia, A. Nocera, G. A. Sawatzky, and A. de la Torre for illuminating discussions.

Appendix A: Cluster Calculations

Ground State. At half-filling, the cluster's ground state can be written as a linear combination of the states

$$|d^1\underline{L}^0\rangle = p^\dagger_{L\uparrow}p^\dagger_{L\downarrow}d^\dagger_\uparrow p^\dagger_{R\uparrow}p^\dagger_{R\downarrow}\,|\text{vac}\rangle = |2,\uparrow,2\rangle \tag{A1}$$

and

$$\begin{aligned}|d^2\underline{L}^1\rangle &= \tfrac{1}{\sqrt{2}}\left[p^\dagger_{L,\uparrow}d^\dagger_\uparrow d^\dagger_\downarrow p^\dagger_{R\uparrow}p^\dagger_{R\downarrow} - p^\dagger_{L,\uparrow}p^\dagger_{L,\downarrow}d^\dagger_\uparrow d^\dagger_\downarrow p^\dagger_{R\uparrow}\right]|\text{vac}\rangle \\ &= \tfrac{1}{\sqrt{2}}\left[|\uparrow,2,2\rangle - |2,2,\uparrow\rangle\right].\end{aligned} \tag{A2}$$

In these expressions, the operators $p^\dagger_{L/R,\sigma}$ create an electron with spin σ on the left (L)/right (R) p orbitals of the cluster, while $d^\dagger_\sigma$ does the same on the central d orbital. We only introduce this notation here to define the normal ordering of the operators. In this sector, the Hamiltonian is represented by the 2×2 matrix

$$H_0 = \begin{pmatrix}\Delta & \sqrt{2}t\\ \sqrt{2}t & U\end{pmatrix}, \tag{A3}$$

yielding the ground state energy

$$E_0 = \left(\frac{\Delta+U}{2}\right) - \sqrt{\left(\frac{\Delta-U}{2}\right)^2 - 2t^2}. \tag{A4}$$

Excitations with one hole. The Fock space with one additional hole and $S^z_{\rm tot} = 0$ is spanned by the states

$$\begin{aligned}
|d^0\underline{\rm L}^0\rangle &= |2,0,2\rangle\,,\\
|\overline{220}\pm\rangle &= \tfrac{1}{\sqrt{2}}\left[|2,2,0\rangle \pm |0,2,2\rangle\right],\\
|\overline{\downarrow 2\uparrow}\pm\rangle &= \tfrac{1}{\sqrt{2}}\left[|\downarrow,2,\uparrow\rangle \pm |\uparrow,2,\downarrow\rangle\right],\\
|\overline{2\uparrow\downarrow}\pm\rangle &= \tfrac{1}{\sqrt{2}}\left[|2,\uparrow,\downarrow\rangle \mp |\downarrow,\uparrow,2\rangle\right], \text{ and}\\
|\overline{2\downarrow\uparrow}\pm\rangle &= \tfrac{1}{\sqrt{2}}\left[|2,\downarrow,\uparrow\rangle \mp |\uparrow,\downarrow,2\rangle\right],
\end{aligned} \tag{A5}$$

where the $+(-)$ sign corresponds to the symmetric (antisymmetric) sector under reflections about the central site. The $|d^0\underline{\rm L}^0\rangle$ state is symmetric, and the states $|\overline{220}\pm\rangle$ are triplet (+) or singlet (-) states. In addition, the linear combinations $|\overline{2\uparrow\downarrow}\pm\rangle \pm |\overline{2\downarrow\uparrow}\pm\rangle$ yield symmetric and anti-symmetric singlet (-) or triplet (-) wavefunctions.

The Hamiltonian matrices for the two sectors are:

$$H_+ = \begin{pmatrix}
-2\Delta & 0 & 0 & -\sqrt{2}t & \sqrt{2}t\\
0 & U & 0 & -t & t\\
0 & 0 & U & -t & t\\
-\sqrt{2}t & -t & -t & -\Delta & 0\\
\sqrt{2}t & t & t & 0 & -\Delta
\end{pmatrix} \tag{A6}$$

and

$$H_- = \begin{pmatrix}
U & 0 & t, & -t\\
0 & U & -t & -t\\
t & -t & -\Delta & 0\\
-t & -t & 0 & -\Delta
\end{pmatrix}, \tag{A7}$$

which can be solved numerically to obtain the eigenvalue spectrum plotted in Fig. 2.

[1] C. N. R. Rao, Transition metal oxides, Annual Review of Physical Chemistry **40**, 291 (1989).

[2] M. Imada, A. Fujimori, and Y. Tokura, Metal-insulator transitions, Rev. Mod. Phys. **70**, 1039 (1998).

[3] J. Ngai, F. Walker, and C. Ahn, Correlated oxide physics and electronics, Annual Review of Materials Research **44**, 1 (2014).

[4] J. Chakhalian, J. W. Freeland, A. J. Millis, C. Panagopoulos, and J. M. Rondinelli, Colloquium: Emergent properties in plane view: Strong correlations at oxide interfaces, Rev. Mod. Phys. **86**, 1189 (2014).

[5] J. Zaanen, G. A. Sawatzky, and J. W. Allen, Band gaps and electronic structure of transition-metal compounds, Phys. Rev. Lett. **55**, 418 (1985).

[6] S. Catalano, M. Gibert, J. Fowlie, J. Íñiguez, J.-M. Triscone, and J. Kreisel, Rare-earth nickelates $RNiO_3$: thin films and heterostructures, Reports on Progress in Physics **81**, 046501 (2018).

[7] M. Bibes, J. E. Villegas, and A. Barthélémy, Ultrathin oxide films and interfaces for electronics and spintronics, Advances in Physics **60**, 5 (2011).

[8] H. Y. Hwang, Y. Iwasa, M. Kawasaki, B. Keimer, N. Nagaosa, and Y. Tokura, Emergent phenomena at oxide interfaces, Nature Materials **11**, 103 (2012).

[9] J. Mannhart and D. G. Schlom, Oxide interfaces—an opportunity for electronics, Science **327**, 1607 (2010).

[10] H. Chen and A. Millis, Charge transfer driven emergent phenomena in oxide heterostructures, Journal of Physics: Condensed Matter **29**, 243001 (2017).

[11] D. I. Khomskii, Unusual valence, negative charge-transfer gaps and self-doping in transition-metal compounds, Lithuanian J. Phys. **37**, 65 (1997), Preprint available at https://arxiv.org/abs/cond-mat/0101164.

[12] R. J. Green and G. A. Sawatzky, Negative charge transfer energy in correlated compounds, Journal of the Physical Society of Japan **93**, 121007 (2024).

[13] T. Mizokawa, H. Namatame, A. Fujimori, K. Akeyama, H. Kondoh, H. Kuroda, and N. Kosugi, Origin of the band gap in the negative charge-transfer-energy compound $NaCuO_2$, Phys. Rev. Lett. **67**, 1638 (1991).

[14] V. Bisogni, S. Catalano, R. J. Green, M. Gibert, R. Scherwitzl, Y. Huang, V. N. Strocov, P. Zubko, S. Balandeh, J.-M. Triscone, G. Sawatzky, and T. Schmitt, Ground-state oxygen holes and the metal–insulator transition in the negative charge-transfer rare-earth nickelates, Nature Communications **7**, 13017 (2016).

[15] N. C. Plumb, D. J. Gawryluk, Y. Wang, Z. Ristić, J. Park, B. Q. Lv, Z. Wang, C. E. Matt, N. Xu, T. Shang, K. Conder, J. Mesot, S. Johnston, M. Shi, and M. Radović, Momentum-resolved electronic structure of the high-T_c superconductor parent compound $BaBiO_3$, Phys. Rev. Lett. **117**, 037002 (2016).

[16] T. Akao, Y. Azuma, M. Usuda, Y. Nishihata, J. Mizuki, N. Hamada, N. Hayashi, T. Terashima, and M. Takano, Charge-ordered state in single-crystalline $CaFeO_3$ thin film studied by x-ray anomalous diffraction, Phys. Rev. Lett. **91**, 156405 (2003).

[17] P. W. Anderson, Antiferromagnetism. Theory of superexchange interaction, Phys. Rev. **79**, 350 (1950).

[18] P. W. Anderson, New approach to the theory of superexchange interactions, Phys. Rev. **115**, 2 (1959).

[19] P. W. Anderson, Exchange in insulators: Superexchange, direct exchange, and double exchange, in *Magnetism I* (Academic Press, New York, 1963) pp. 25–85.

[20] J. Zaanen and G. A. Sawatzky, The electronic structure

and superexchange interactions in transition-metal compounds, Canadian Journal of Physics **65**, 1262 (1987).
[21] H. Eskes, L. H. Tjeng, and G. A. Sawatzky, Cluster-model calculation of the electronic structure of CuO: A model material for the high-T_c superconductors, Phys. Rev. B **41**, 288 (1990).
[22] D. Li, K. Lee, B. Y. Wang, M. Osada, S. Crossley, H. R. Lee, Y. Cui, Y. Hikita, and H. Y. Hwang, Superconductivity in an infinite-layer nickelate, Nature **572**, 624 (2019).
[23] G. A. Pan, D. Ferenc Segedin, H. LaBollita, Q. Song, E. M. Nica, B. H. Goodge, A. T. Pierce, S. Doyle, S. Novakov, D. Córdova Carrizales, A. T. N'Diaye, P. Shafer, H. Paik, J. T. Heron, J. A. Mason, A. Yacoby, L. F. Kourkoutis, O. Erten, C. M. Brooks, A. S. Botana, and J. A. Mundy, Superconductivity in a quintuple-layer square-planar nickelate, Nature Materials **21**, 160 (2022).
[24] H. Sun, M. Huo, X. Hu, J. Li, Z. Liu, Y. Han, L. Tang, Z. Mao, P. Yang, B. Wang, J. Cheng, D.-X. Yao, G.-M. Zhang, and M. Wang, Signatures of superconductivity near 80 K in a nickelate under high pressure, Nature **621**, 493 (2023).
[25] B. Y. Wang, K. Lee, and B. H. Goodge, Experimental progress in superconducting nickelates, Annual Review of Condensed Matter Physics **15**, 305 (2024).
[26] L.-H. Hu and C. Wu, Two-band model for magnetism and superconductivity in nickelates, Phys. Rev. Res. **1**, 032046 (2019).
[27] Y. Nomura, M. Hirayama, T. Tadano, Y. Yoshimoto, K. Nakamura, and R. Arita, Formation of a two-dimensional single-component correlated electron system and band engineering in the nickelate superconductor $NdNiO_2$, Phys. Rev. B **100**, 205138 (2019).
[28] M. Jiang, M. Moeller, M. Berciu, and G. A. Sawatzky, Relevance of Cu − 3d multiplet structure in models of high-T_c cuprates, Phys. Rev. B **101**, 035151 (2020).
[29] Y. Gu, S. Zhu, X. Wang, J. Hu, and H. Chen, A substantial hybridization between correlated Ni-d orbital and itinerant electrons in infinite-layer nickelates, Communications Physics **3**, 84 (2020).
[30] H. Sakakibara, H. Usui, K. Suzuki, T. Kotani, H. Aoki, and K. Kuroki, Model construction and a possibility of cupratelike pairing in a new d^9 nickelate superconductor (Nd, Sr)NiO_2, Phys. Rev. Lett. **125**, 077003 (2020).
[31] M. Hepting, D. Li, C. J. Jia, H. Lu, E. Paris, Y. Tseng, X. Feng, M. Osada, E. Been, Y. Hikita, Y. D. Chuang, Z. Hussain, K. J. Zhou, A. Nag, M. Garcia-Fernandez, M. Rossi, H. Y. Huang, D. J. Huang, Z. X. Shen, T. Schmitt, H. Y. Hwang, B. Moritz, J. Zaanen, T. P. Devereaux, and W. S. Lee, Electronic structure of the parent compound of superconducting infinite-layer nickelates, Nature Materials **19**, 381 (2020).
[32] P. Adhikary, S. Bandyopadhyay, T. Das, I. Dasgupta, and T. Saha-Dasgupta, Orbital-selective superconductivity in a two-band model of infinite-layer nickelates, Phys. Rev. B **102**, 100501 (2020).
[33] B.-X. Wang, H. Zheng, E. Krivyakina, O. Chmaissem, P. P. Lopes, J. W. Lynn, L. C. Gallington, Y. Ren, S. Rosenkranz, J. F. Mitchell, and D. Phelan, Synthesis and characterization of bulk $Nd_{1-x}Sr_xNiO_2$ and $Nd_{1-x}Sr_xNiO_3$, Phys. Rev. Mater. **4**, 084409 (2020).
[34] A. S. Botana and M. R. Norman, Similarities and differences between $LaNiO_2$ and $CaCuO_2$ and implications for superconductivity, Phys. Rev. X **10**, 011024 (2020).
[35] F. Lechermann, Doping-dependent character and possible magnetic ordering of $NdNiO_2$, Phys. Rev. Mater. **5**, 044803 (2021).
[36] F. Petocchi, V. Christiansson, F. Nilsson, F. Aryasetiawan, and P. Werner, Normal state of $Nd_{1-x}Sr_xNiO_2$ from self-consistent GW + EDMFT, Phys. Rev. X **10**, 041047 (2020).
[37] J. Karp, A. S. Botana, M. R. Norman, H. Park, M. Zingl, and A. Millis, Many-body electronic structure of $NdNiO_2$ and $CaCuO_2$, Phys. Rev. X **10**, 021061 (2020).
[38] Y. Shen, J. Sears, G. Fabbris, J. Li, J. Pelliciari, I. Jarrige, X. He, I. Božović, M. Mitrano, J. Zhang, J. F. Mitchell, A. S. Botana, V. Bisogni, M. R. Norman, S. Johnston, and M. P. M. Dean, Role of oxygen states in the low valence nickelate $La_4Ni_3O_8$, Phys. Rev. X **12**, 011055 (2022).
[39] H. Park, A. J. Millis, and C. A. Marianetti, Site-selective Mott transition in rare-earth-element nickelates, Phys. Rev. Lett. **109**, 156402 (2012).
[40] S. Johnston, A. Mukherjee, I. Elfimov, M. Berciu, and G. A. Sawatzky, Charge disproportionation without charge transfer in the rare-earth-element nickelates as a possible mechanism for the metal-insulator transition, Phys. Rev. Lett. **112**, 106404 (2014).
[41] A. Khazraie, K. Foyevtsova, I. Elfimov, and G. A. Sawatzky, Oxygen holes and hybridization in the bismuthates, Phys. Rev. B **97**, 075103 (2018).
[42] B. Cohen-Stead, K. Barros, R. Scalettar, and S. Johnston, A hybrid Monte Carlo study of bond-stretching electron–phonon interactions and charge order in $BaBiO_3$, npj Computational Materials **9**, 40 (2023).
[43] J. Shamblin, M. Heres, H. Zhou, J. Sangoro, M. Lang, J. Neuefeind, J. A. Alonso, and S. Johnston, Experimental evidence for bipolaron condensation as a mechanism for the metal-insulator transition in rare-earth nickelates, Nature Communications **9**, 86 (2018).
[44] M. Tyunina, M. Savinov, O. Pacherova, and A. Dejneka, Small-polaron transport in perovskite nickelates, Scientific Reports **13**, 12493 (2023).
[45] W. Pickett, The other high-temperature superconductors, Physica B: Condensed Matter **296**, 112 (2001).
[46] A. W. Sleight, Bismuthates: $BaBiO_3$ and related superconducting phases, Physica C: Superconductivity and its Applications **514**, 152 (2015).
[47] M. Kim, G. M. McNally, H.-H. Kim, M. Oudah, A. S. Gibbs, P. Manuel, R. J. Green, R. Sutarto, T. Takayama, A. Yaresko, U. Wedig, M. Isobe, R. K. Kremer, D. A. Bonn, B. Keimer, and H. Takagi, Superconductivity in (Ba,K)SbO_3, Nature Materials **21**, 627 (2022).
[48] G. A. Sawatzky and J. W. Allen, Magnitude and origin of the band gap in NiO, Phys. Rev. Lett. **53**, 2339 (1984).
[49] T. Mizokawa, A. Fujimori, H. Namatame, K. Akeyama, and N. Kosugi, Electronic structure of the local-singlet insulator $NaCuO_2$, Phys. Rev. B **49**, 7193 (1994).
[50] M. W. Haverkort, M. Zwierzycki, and O. K. Andersen, Multiplet ligand-field theory using Wannier orbitals, Phys. Rev. B **85**, 165113 (2012).
[51] T. Mizokawa, D. I. Khomskii, and G. A. Sawatzky, Spin and charge ordering in self-doped Mott insulators, Phys. Rev. B **61**, 11263 (2000).

[52] T. Yamaguchi, K. Higashi, A. Regoutz, Y. Takahashi, M. Lazemi, Q. Che, F. M. F. de Groot, and A. Hariki, Atomic multiplet and charge transfer screening effects in 1s and 2p core-level x-ray photoelectron spectra of early 3d transition-metal oxides, Phys. Rev. B **109**, 205143 (2024).

[53] M. W. Haverkort, Quanty for core level spectroscopy - excitons, resonances and band excitations in time and frequency domain, Journal of Physics: Conference Series **712**, 012001 (2016).

[54] J. W. Freeland, M. van Veenendaal, and J. Chakhalian, Evolution of electronic structure across the rare-earth $RNiO_3$ series, Journal of Electron Spectroscopy and Related Phenomena **208**, 56 (2016).

[55] C.-C. Chen, M. Sentef, Y. F. Kung, C. J. Jia, R. Thomale, B. Moritz, A. P. Kampf, and T. P. Devereaux, Doping evolution of the oxygen K-edge x-ray absorption spectra of cuprate superconductors using a three-orbital Hubbard model, Phys. Rev. B **87**, 165144 (2013).

[56] A. Dobry, A. Greco, J. Lorenzana, and J. Riera, Polarons in the three-band Peierls-Hubbard model: An exact diagonalization study, Phys. Rev. B **49**, 505 (1994).

[57] B. Lau, M. Berciu, and G. A. Sawatzky, High-spin polaron in lightly doped CuO_2 planes, Phys. Rev. Lett. **106**, 036401 (2011).

[58] B. Lau, M. Berciu, and G. A. Sawatzky, Computational approach to a doped antiferromagnet: Correlations between two spin polarons in the lightly doped CuO_2 plane, Phys. Rev. B **84**, 165102 (2011).

[59] S. Li, A. Nocera, U. Kumar, and S. Johnston, Particle-hole asymmetry in the dynamical spin and charge responses of corner-shared 1D cuprates, Communications Physics **4**, 217 (2021).

[60] A. Nocera, U. Kumar, N. Kaushal, G. Alvarez, E. Dagotto, and S. Johnston, Computing resonant inelastic x-ray scattering spectra using the density matrix renormalization group method, Scientific Reports **8**, 11080 (2018).

[61] S. R. White and D. J. Scalapino, Doping asymmetry and striping in a three-orbital CuO_2 Hubbard model, Phys. Rev. B **92**, 205112 (2015).

[62] M. Guerrero, J. E. Gubernatis, and S. Zhang, Quantum Monte Carlo study of hole binding and pairing correlations in the three-band Hubbard model, Phys. Rev. B **57**, 11980 (1998).

[63] A. Chiciak, E. Vitali, H. Shi, and S. Zhang, Magnetic orders in the hole-doped three-band Hubbard model: Spin spirals, nematicity, and ferromagnetic domain walls, Phys. Rev. B **97**, 235127 (2018).

[64] E. W. Huang, C. B. Mendl, S. Liu, S. Johnston, H. C. Jiang, B. Moritz, and T. P. Devereaux, Numerical evidence of fluctuating stripes in the normal state of high-T_c cuprate superconductors, Science **358**, 1161–1164 (2017).

[65] P. Mai, B. Cohen-Stead, T. A. Maier, and S. Johnston, Fluctuating charge-density-wave correlations in the three-band Hubbard model, Proceedings of the National Academy of Sciences **121**, e2408717121 (2024).

[66] C. Weber, C. Yee, K. Haule, and G. Kotliar, Scaling of the transition temperature of hole-doped cuprate superconductors with the charge-transfer energy, Europhysics Letters **100**, 37001 (2012).

[67] P. Mai, G. Balduzzi, S. Johnston, and T. A. Maier, Orbital structure of the effective pairing interaction in the high-temperature superconducting cuprates, npj Quantum Materials **6**, 26 (2021).

[68] Z.-H. Cui, C. Sun, U. Ray, B.-X. Zheng, Q. Sun, and G. K.-L. Chan, Ground-state phase diagram of the three-band Hubbard model from density matrix embedding theory, Phys. Rev. Res. **2**, 043259 (2020).

[69] E. Dagotto, Correlated electrons in high-temperature superconductors, Rev. Mod. Phys. **66**, 763 (1994).

[70] D. Scalapino, Numerical studies of the 2D Hubbard model, in *Handbook of High-Temperature Superconductivity*, edited by J. Schrieffer and J. Brooks (Springer New York, 2007) pp. 495–526.

[71] M. Qin, T. Schäfer, S. Andergassen, P. Corboz, and E. Gull, The Hubbard model: A computational perspective, Annual Review of Condensed Matter Physics **13**, 275 (2022).

[72] J. P. F. LeBlanc, A. E. Antipov, F. Becca, I. W. Bulik, G. K.-L. Chan, C.-M. Chung, Y. Deng, M. Ferrero, T. M. Henderson, C. A. Jiménez-Hoyos, E. Kozik, X.-W. Liu, A. J. Millis, N. V. Prokof'ev, M. Qin, G. E. Scuseria, H. Shi, B. V. Svistunov, L. F. Tocchio, I. S. Tupitsyn, S. R. White, S. Zhang, B.-X. Zheng, Z. Zhu, and E. Gull (Simons Collaboration on the Many-Electron Problem), Solutions of the two-dimensional Hubbard model: Benchmarks and results from a wide range of numerical algorithms, Phys. Rev. X **5**, 041041 (2015).

[73] M. Qin, C.-M. Chung, H. Shi, E. Vitali, C. Hubig, U. Schollwöck, S. R. White, and S. Zhang (Simons Collaboration on the Many-Electron Problem), Absence of superconductivity in the pure two-dimensional Hubbard model, Phys. Rev. X **10**, 031016 (2020).

[74] F. C. Zhang and T. M. Rice, Effective Hamiltonian for the superconducting Cu oxides, Phys. Rev. B **37**, 3759 (1988).

[75] H.-B. Schüttler and A. J. Fedro, Copper-oxygen charge excitations and the effective-single-band theory of cuprate superconductors, Phys. Rev. B **45**, 7588 (1992).

[76] M. Simon, M. Balina, and A. Aligia, Effective one-band Hamiltonian for cuprate superconductor metal-insulator transition, Physica C: Superconductivity **206**, 297 (1993).

[77] M. E. Simón and A. A. Aligia, Brinkman-Rice transition in layered perovskites, Phys. Rev. B **48**, 7471 (1993).

[78] L. F. Feiner, J. H. Jefferson, and R. Raimondi, Effective single-band models for the high-T_c cuprates. I. Coulomb interactions, Phys. Rev. B **53**, 8751 (1996).

[79] V. I. Belinicher, A. L. Chernyshev, and L. V. Popovich, Range of the t-J model parameters for CuO_2 planes: Experimental data constraints, Phys. Rev. B **50**, 13768 (1994).

[80] V. I. Belinicher and A. L. Chernyshev, Consistent low-energy reduction of the three-band model for copper oxides with O-O hopping to the effective t-J model, Phys. Rev. B **49**, 9746 (1994).

[81] A. A. Aligia, M. E. Simón, and C. D. Batista, Systematic derivation of a generalized t-J model, Phys. Rev. B **49**, 13061 (1994).

[82] H. Ebrahimnejad, G. A. Sawatzky, and M. Berciu, The dynamics of a doped hole in a cuprate is not controlled by spin fluctuations, Nature Physics **10**, 951 (2014).

[83] I. J. Hamad, L. O. Manuel, and A. A. Aligia, Magnon-assisted dynamics of a hole doped in a cuprate super-

conductor, Phys. Rev. B **103**, 144510 (2021).
[84] C. P. J. Adolphs, S. Moser, G. A. Sawatzky, and M. Berciu, Non-Zhang-Rice singlet character of the first ionization state of T-CuO, Phys. Rev. Lett. **116**, 087002 (2016).
[85] I. J. Hamad, L. O. Manuel, and A. A. Aligia, Generalized one-band model based on Zhang-Rice singlets for tetragonal CuO, Phys. Rev. Lett. **120**, 177001 (2018).
[86] A. A. Aligia, Comment on "Relevance of Cu-3d multiplet structure in models of high-T_c cuprates", Phys. Rev. B **102**, 117101 (2020).
[87] I. Santoso, W. Ku, T. Shirakawa, G. Neuber, X. Yin, M. Enoki, M. Fujita, R. Liang, T. Venkatesan, G. A. Sawatzky, A. Kotlov, S. Yunoki, M. Rübhausen, and A. Rusydi, Unraveling local spin polarization of Zhang-Rice singlet in lightly hole-doped cuprates using high-energy optical conductivity, Phys. Rev. B **95**, 165108 (2017).
[88] K. Penc and W. Stephan, Dynamical correlations in one-dimensional charge-transfer insulators, Physical Review B **62**, 12707 (2000).
[89] R. Neudert, S.-L. Drechsler, J. Málek, H. Rosner, M. Kielwein, Z. Hu, M. Knupfer, M. S. Golden, J. Fink, N. Nücker, M. Merz, S. Schuppler, N. Motoyama, H. Eisaki, S. Uchida, M. Domke, and G. Kaindl, Four-band extended Hubbard Hamiltonian for the one-dimensional cuprate Sr_2CuO_3 : distribution of oxygen holes and its relation to strong intersite Coulomb interaction, Phys. Rev. B **62**, 10752 (2000).
[90] C. Kim, A. Y. Matsuura, Z.-X. Shen, N. Motoyama, H. Eisaki, S. Uchida, T. Tohyama, and S. Maekawa, Observation of spin-charge separation in one-dimensional $SrCuO_2$, Phys. Rev. Lett. **77**, 4054 (1996).
[91] K. M. Kojima, Y. Fudamoto, M. Larkin, G. M. Luke, J. Merrin, B. Nachumi, Y. J. Uemura, N. Motoyama, H. Eisaki, S. Uchida, K. Yamada, Y. Endoh, S. Hosoya, B. J. Sternlieb, and G. Shirane, Reduction of ordered moment and Néel temperature of quasi-one-dimensional antiferromagnets Sr_2CuO_3 and Ca_2CuO_3, Phys. Rev. Lett. **78**, 1787 (1997).
[92] H. Eisaki, N. Motoyama, and S. Uchida, Spin magnetic susceptibility of Cu-O chains in Sr_2CuO_3 and $SrCuO_2$, Physica C: Superconductivity **282-287**, 1323 (1997).
[93] I. A. Zaliznyak, H. Woo, T. G. Perring, C. L. Broholm, C. D. Frost, and H. Takagi, Spinons in the strongly correlated copper oxide chains in $SrCuO_2$, Phys. Rev. Lett. **93**, 087202 (2004).
[94] B. J. Kim, H. Koh, E. Rotenberg, S. J. Oh, H. Eisaki, N. Motoyama, S. Uchida, T. Tohyama, S. Maekawa, Z. X. Shen, and C. Kim, Distinct spinon and holon dispersions in photoemission spectral functions from one-dimensional $SrCuO_2$, Nature Physics **2**, 397 (2006).
[95] M. Enderle, B. Fåk, H.-J. Mikeska, R. K. Kremer, A. Prokofiev, and W. Assmus, Two-spinon and four-spinon continuum in a frustrated ferromagnetic spin-1/2 chain, Phys. Rev. Lett. **104**, 237207 (2010).
[96] S.-L. Drechsler, S. Nishimoto, R. O. Kuzian, J. Málek, W. E. A. Lorenz, J. Richter, J. van den Brink, M. Schmitt, and H. Rosner, Comment on "two-spinon and four-spinon continuum in a frustrated ferromagnetic spin-1/2 chain", Phys. Rev. Lett. **106**, 219701 (2011).
[97] J. Schlappa, K. Wohlfeld, K. J. Zhou, M. Mourigal, M. W. Haverkort, V. N. Strocov, L. Hozoi, C. Monney, S. Nishimoto, S. Singh, A. Revcolevschi, J. S. Caux, L. Patthey, H. M. Rønnow, J. van den Brink, and T. Schmitt, Spin–orbital separation in the quasi-one-dimensional Mott insulator Sr_2CuO_3, Nature **485**, 82 (2012).
[98] V. Bisogni, S. Kourtis, C. Monney, K. Zhou, R. Kraus, C. Sekar, V. Strocov, B. Büchner, J. van den Brink, L. Braicovich, T. Schmitt, M. Daghofer, and J. Geck, Femtosecond dynamics of momentum-dependent magnetic excitations from resonant inelastic x-ray scattering in $CaCu_2O_3$, Phys. Rev. Lett. **112**, 147401 (2014).
[99] A. C. Walters, T. G. Perring, J.-S. Caux, A. T. Savici, G. D. Gu, C.-C. Lee, W. Ku, and I. A. Zaliznyak, Effect of covalent bonding on magnetism and the missing neutron intensity in copper oxide compounds, Nature Physics **5**, 867 (2009).
[100] D. Bounoua, R. Saint-Martin, J. Dai, T. Rödel, S. Sengupta, E. Frantzeskakis, F. Bertran, P. Lefevre, F. Fortuna, A. F. Santander-Syro, and L. Pinsard-Gaudart, Angle resolved photoemission spectroscopy study of the spin-charge separation in the strongly correlated cuprates $SrCuO_2$ and Sr_2CuO_3 with $S = 0$ impurities, Journal of Electron Spectroscopy and Related Phenomena **225**, 49 (2018).
[101] J. Schlappa, U. Kumar, K. J. Zhou, S. Singh, M. Mourigal, V. N. Strocov, A. Revcolevschi, L. Patthey, H. M. Rønnow, S. Johnston, and T. Schmitt, Probing multi-spinon excitations outside of the two-spinon continuum in the antiferromagnetic spin chain cuprate Sr_2CuO_3, Nature Communications **9**, 5394 (2018).
[102] U. Kumar, A. Nag, J. Li, H. C. Robarts, A. C. Walters, M. García-Fernández, R. Saint-Martin, A. Revcolevschi, J. Schlappa, T. Schmitt, S. Johnston, and K.-J. Zhou, Unraveling higher-order contributions to spin excitations probed using resonant inelastic x-ray scattering, Phys. Rev. B **106**, L060406 (2022).
[103] Z. Chen, Y. Wang, S. N. Rebec, T. Jia, M. Hashimoto, D. Lu, B. Moritz, R. G. Moore, T. P. Devereaux, and Z.-X. Shen, Anomalously strong near-neighbor attraction in doped 1D cuprate chains, Science **373**, 1235 (2021).
[104] J. Li, D. Jost, T. Tang, R. Wang, Y. Zhong, Z. Chen, M. Garcia-Fernandez, J. Pelliciari, V. Bisogni, B. Moritz, K. Zhou, Y. Wang, T. P. Devereaux, W.-S. Lee, and Z.-X. Shen, Doping dependence of 2-spinon excitations in the doped 1D cuprate $Ba_2CuO_{3+\delta}$, Phys. Rev. Lett. **134**, 146501 (2025).
[105] Y. Wang, Z. Chen, T. Shi, B. Moritz, Z.-X. Shen, and T. P. Devereaux, Phonon-mediated long-range attractive interaction in one-dimensional cuprates, Phys. Rev. Lett. **127**, 197003 (2021).
[106] T. Tang, B. Moritz, C. Peng, Z.-X. Shen, and T. P. Devereaux, Traces of electron-phonon coupling in one-dimensional cuprates, Nature Communications **14**, 3129 (2023).
[107] H.-X. Wang, Y.-M. Wu, Y.-F. Jiang, and H. Yao, Spectral properties of 1D extended Hubbard model from bosonization and time-dependent variational principle: applications to 1D cuprate, arXiv:2211.02031 (2022).
[108] U. Kumar, A. Nocera, E. Dagotto, and S. Johnston, Multi-spinon and antiholon excitations probed by resonant inelastic x-ray scattering on doped one-dimensional antiferromagnets, New Journal of Physics **20**, 073019 (2018).
[109] A. E. Feiguin, C. Helman, and A. A. Aligia, Effec-

tive one-band models for the one-dimensional cuprate $Ba_{2-x}Sr_xCuO_{3+\delta}$, Phys. Rev. B **108**, 075125 (2023).
[110] J. Zaanen and A. M. Oleś, Canonical perturbation theory and the two-band model for high-T_c superconductors, Phys. Rev. B **37**, 9423 (1988).
[111] K. Okada and A. Kotani, Intersite Coulomb interactions in quasi-one-dimensional copper oxides, Journal of the Physical Society of Japan **66**, 341 (1997), https://doi.org/10.1143/JPSJ.66.341.
[112] K. Maiti, D. D. Sarma, T. Mizokawa, and A. Fujimori, Electronic structure of one-dimensional cuprates, Phys. Rev. B **57**, 1572 (1998).
[113] K. Wohlfeld, S. Nishimoto, M. W. Haverkort, and J. van den Brink, Microscopic origin of spin-orbital separation in Sr_2CuO_3, Phys. Rev. B **88**, 195138 (2013).
[114] C. Monney, V. Bisogni, K.-J. Zhou, R. Kraus, V. N. Strocov, G. Behr, J. c. v. Málek, R. Kuzian, S.-L. Drechsler, S. Johnston, A. Revcolevschi, B. Büchner, H. M. Rønnow, J. van den Brink, J. Geck, and T. Schmitt, Determining the short-range spin correlations in the spin-chain Li_2CuO_2 and $CuGeO_3$ compounds using resonant inelastic x-ray scattering, Phys. Rev. Lett. **110**, 087403 (2013).
[115] A. Chainani, M. Horio, C.-M. Cheng, D. Malterre, K. Sheshadri, M. Kobayashi, K. Horiba, H. Kumigashira, T. Mizokawa, M. Oura, M. Taguchi, Y. Mori, A. Takahashi, T. Konno, T. Ohgi, H. Sato, T. Adachi, Y. Koike, T. Mochiku, K. Hirata, S. Shin, M. K. Wu, and A. Fujimori, Oxygen on-site Coulomb energy in $Pr_{1.3-x}La_{0.7}Ce_xCuO_4$ and $Bi_2Sr_2CaCu_2O_{8+\delta}$ and its relation with Heisenberg exchange, Phys. Rev. B **107**, 195152 (2023).
[116] C. Varma, S. Schmitt-Rink, and E. Abrahams, Charge transfer excitations and superconductivity in "ionic" metals, Solid State Communications **88**, 847 (1993).
[117] S. R. White and A. E. Feiguin, Real-time evolution using the density matrix renormalization group, Phys. Rev. Lett. **93**, 076401 (2004).
[118] A. J. Daley, C. Kollath, U. Schollwöck, and G. Vidal, Time-dependent density-matrix renormalization-group using adaptive effective Hilbert spaces, Journal of Statistical Mechanics: Theory and Experiment **2004**, P04005 (2004).
[119] A. E. Feiguin, The density matrix renormalization group method and its time-dependent variants, in *XV Training Course in the Physics of Strongly Correlated Systems*, Vol. 1419 (AIP Proceedings, 2011) p. 5.
[120] S. Paeckel, T. Köhler, A. Swoboda, S. R. Manmana, U. Schollwöck, and C. Hubig, Time-evolution methods for matrix-product states, Annals of Physics **411**, 167998 (2019).
[121] K. Zawadzki, A. Nocera, and A. E. Feiguin, A time-dependent momentum-resolved scattering approach to core-level spectroscopies, SciPost Phys. **15**, 166 (2023).
[122] A. V. Oppenheim, R. W. Schafer, and J. R. Buck, *Discrete-Time Signal Processing*, 2nd ed. (Prentice-hall Englewood Cliffs, 1999).
[123] M. Ogata and H. Shiba, Bethe-ansatz wave function, momentum distribution, and spin correlation in the one-dimensional strongly correlated Hubbard model, Phys. Rev. B **41**, 2326 (1990).
[124] K. Penc, K. Hallberg, F. Mila, and H. Shiba, Spectral functions of the one-dimensional Hubbard model in the $U \to +\infty$ limit: How to use the factorized wave function, Phys. Rev. B **55**, 15475 (1997).
[125] H. Benthien and E. Jeckelmann, Spin and charge dynamics of the one-dimensional extended Hubbard model, Phys. Rev. B **75**, 205128 (2007).
[126] F. de Groot and A. Kotani, *Core Level Spectroscopy of Solids* (CRC Press, Boca Raton, FL, 2008).
[127] C. T. Chantler, G. Bunker, P. D'Angelo, and S. Diaz-Moreno, X-ray absorption spectroscopy, Nature Reviews Methods Primers **4**, 89 (2024).
[128] Nocera, Alberto and Feiguin, Adrian, Auger spectroscopy beyond the ultra-short core-hole relaxation time approximation, Eur. Phys. J. Plus **138**, 1106 (2023).
[129] P. Bourges, H. Casalta, A. S. Ivanov, and D. Petitgrand, Superexchange coupling and spin susceptibility spectral weight in undoped monolayer cuprates, Phys. Rev. Lett. **79**, 4906 (1997).
[130] R. Coldea, S. M. Hayden, G. Aeppli, T. G. Perring, C. D. Frost, T. E. Mason, S.-W. Cheong, and Z. Fisk, Spin waves and electronic interactions in La_2CuO_4, Phys. Rev. Lett. **86**, 5377 (2001).
[131] J. Lorenzana, G. Seibold, and R. Coldea, Sum rules and missing spectral weight in magnetic neutron scattering in the cuprates, Phys. Rev. B **72**, 224511 (2005).
[132] A. C. Walters, T. G. Perring, J.-S. Caux, A. T. Savici, G. D. Gu, C.-C. Lee, W. Ku, and I. A. Zaliznyak, Effect of covalent bonding on magnetism and the missing neutron intensity in copper oxide compounds, Nature Physics **5**, 867 (2009).
[133] H. Eskes, M. B. J. Meinders, and G. A. Sawatzky, Anomalous transfer of spectral weight in doped strongly correlated systems, Phys. Rev. Lett. **67**, 1035 (1991).
[134] C. Jia, K. Wohlfeld, Y. Wang, B. Moritz, and T. P. Devereaux, Using RIXS to uncover elementary charge and spin excitations, Phys. Rev. X **6**, 021020 (2016).
[135] J. Thomas, D. Banerjee, A. Nocera, and S. Johnston, Theory of electron-phonon interactions in extended correlated systems probed by resonant inelastic x-ray scattering, Phys. Rev. X **15**, 021030 (2025).
[136] P. Laurell, A. Scheie, D. A. Tennant, S. Okamoto, G. Alvarez, and E. Dagotto, Magnetic excitations, nonclassicality, and quantum wake spin dynamics in the Hubbard chain, Phys. Rev. B **106**, 085110 (2022).
[137] A. Scheie, P. Laurell, W. Simeth, E. Dagotto, and D. A. Tennant, Tutorial: Extracting entanglement signatures from neutron spectroscopy, Materials Today Quantum **5**, 100020 (2025).
[138] H. Padma, J. Thomas, S. F. R. TenHuisen, W. He, Z. Guan, J. Li, B. Lee, Y. Wang, S. H. Lee, Z. Mao, H. Jang, V. Bisogni, J. Pelliciari, M. P. M. Dean, S. Johnston, and M. Mitrano, Beyond-Hubbard pairing in a cuprate ladder, Phys. Rev. X **15**, 021049 (2025).
[139] A. Scheie, P. Laurell, J. Thomas, V. Sharma, A. I. Kolesnikov, G. E. Granroth, Q. Zhang, B. Lake, M. M. Jr., R. I. Bewley, R. S. Eccleston, J. Akimitsu, E. Dagotto, C. D. Batista, G. Alvarez, S. Johnston, and D. A. Tennant, Cooper-pair localization in the magnetic dynamics of a cuprate ladder, arXiv:2501.10296 (2025).
[140] S. Milner, A. Feiguin, and S. Johnston, Cu-o chain, 10.5281/zenodo.16876208 (2025).
[141] `https://alps.comp-phys.org`.